Earthquake Engineering, Tenth World Conference © 1992 Balkema, Rotterdam. ISBN 90 5410 060 5

Tests and analyses of ultra-high strength reinforced concrete shear walls

Toshimi Kabeyasawa & Kazuyuki Matsumoto
Yokohama National University, Japan

ABSTRACT : The paper reports the test results of ultra-high strength reinforced concrete shear walls using 600 Mpa and 80 Mpa grade concrete and 700 Mpa and 800 Mpa grade reinforcing steel. Six one-fourth scale shear walls were tested varying the shear span ratio of loading and the reinforcement ratios. Theoretical design equations gave a fair estimation of the observed ultimate flexural and shear strengths. The deformability in web-crushing was related to the residual capacity of the concrete strut in the shear resistance mechanism at flexural yielding.

1 INTRODUCTION

A five-year national research project was started in 1988 in Japan, promoted by the Building Research Institute, Ministry of Construction. The purpose was to investigate on the feasibility of the design and construction of reinforced concrete building structures using ultra-high strength materials, such as concrete up to 120 Mpa and steel up to 1200 Mpa.

Series of experimental and analytical research on ultra-high strength reinforced concrete shear walls were programmed in the project to investigate on the hysteretic behavior and to develop a general design procedure. This experimental research was conducted as a part of the program.

In this study, six one-fourth scale shear walls were tested in two phases. The shear wall assemblies were subjected to relatively high axial load and cyclic lateral shear force. Strength and deformability in a web-crushing mode after flexural yielding are discussed through theoretical calculation.

2 METHOD OF TESTING

2.1 Tested specimens

Tested were six shear wall specimens of about one-fourth scale model, NW-1 through NW-6. The two specimens NW-1 and NW-2 in the first phase were constructed using 80 Mpa grade concrete and 800 Mpa grade steel, while 60 Mpa grade concrete and 600 Mpa grade steel, were used in the four specimens of the second phase, NW-3 through NW-6. The typical reinforcement details (NW-6) are shown in Figure 1.

The six specimens had the same horizontal sectional dimensions: the boundary columns of 20cmx20cm and the wall panel of 8cmx130cm.

The two specimens in the first phase had the same reinforcement details: 12-D10 as the column main bars with sufficient spiral and sub-ties, and 2-D6 at the spacing of 15cm in the wall panel. Only clear height of the wall panel, which corresponded to the shear span of the lateral loading, was varied in the two specimens: 300cm in NW-1 and 200cm in NW-2.

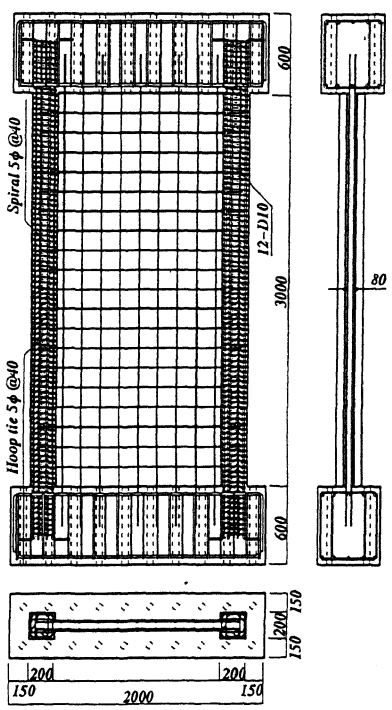

Figure 1 Reinforcement details (NW-6)

Table 1 List of specimens

specimen	height	wall main bar column	wall web bar	axial load[kN]
Phase 1	NW-1 3000 NW-2 2000	12-D10	2-D6@150	1764
Phase 2	NW-3	12-D10	1-D6@150	1372
	NW-4 3000	16-D10	-------	1568
	NW-5	16-D10	2-D6@150	1372
	NW-6	12-D13		1568

	column section(mm)	spiral	sub-tie	wall section
Phase 1 Phase 2	200x200	D6@40 φ5@40	2-D6@40 2-φ5@40	80x1300

Table 2 Material properties

(a) concrete

	specimen	age (days)	compressive strength	tensile strenth	elastic modulus
Phase 1	NW-1	52	87.6 [0.30]	4.58	35600
	NW-2	81	93.6 [0.30]	5.16	37000
Phase 2	NW-3	42	55.5 [0.25]	3.39	33500
	NW-4	47	54.6 [0.25]	3.71	34100
	NW-5	55	60.3 [0.26]	4.18	36200
	NW-6	74	65.2 [0.27]	4.44	35100

unit in MPa, [ ]: strain at compressive strength in percent

(b) steel

	size	area (cm^2)	yield strength	maximum use strength (Mpa)	
Phase 1	D10	0.71	776	996	column main bar
	D6	0.32	1001	1187	wall bar, sub-tie
	D6	0.32	1262	1373	spiral
Phase 2	D13	1.27	726	916	column main bar
	D10	0.71	713	840	column main bar
	D6	0.32	753	952	wall bar
	φ5	0.196	1233	1523	spiral, sub-tie

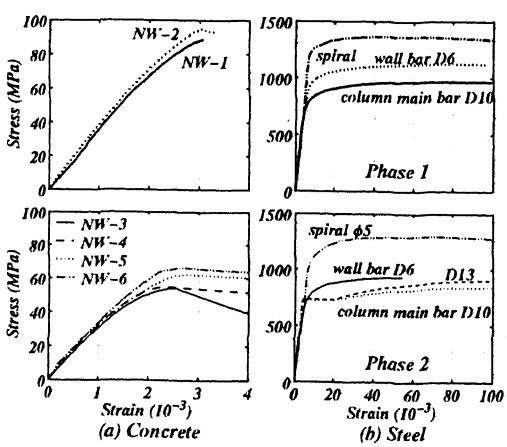

Figure 2 Stress strain relations of concrete and steel

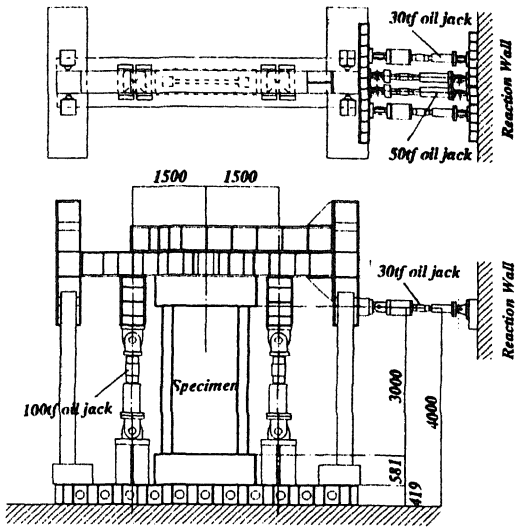

Figure 3 Loading apparatus

The specimens NW-3 through NW-6 in the second phase had the same sectional dimensions with the specimen NW-1. The amount of the longitudinal and lateral reinforcement was varied. The column main bars were 12-D10 in NW-3, 16-D10 in NW-4 and NW-5, 12-D13 in NW-6. The wall panel reinforcing bars were D6 in NW-3 and NW-4, 2-D6 in NW-5 and NW-6 at the spacing of 15cm. Sectional dimensions and reinforcement of all specimens are listed in Table 1.

The material properties of the concrete and reinforcing bars are given in Table 2. The stress-strain relations are shown in Figure 2. Actual strengths of concrete and web reinforcing bars in the first phase were higher than the nominal strengths, while the material properties of the others were satisfactory.

2.1 Loading procedure

The loading set up is shown in Figure 3. The constant amplitude gravity load was applied by two vertical oil jacks to the rigid steel beam attached on the top beam of a specimen. The total axial load levels were corresponded to those at the wall base of about 30 through 40 story building as listed in Table 1.

The cyclic and reversed lateral load was applied through the steel beam at the top level of the wall panel by four horizontal oil jacks attached to the reaction wall. In this loading system, the lateral load point at the center of the specimen changes when the rotation of the steel beam becomes large (P-delta effect). Therefore, in the second phase, the regulating moment was applied by the two vertical jacks in relation to the measured rotation of the beam to keep the shear-span-to-depth ratio constant.

The lateral loading was reversed in two cycles each at the deflection angles R(rad.) of 1/400, 1/200, 1/133, 1/100, 1/67, 1/50, measured at the top of the wall panel

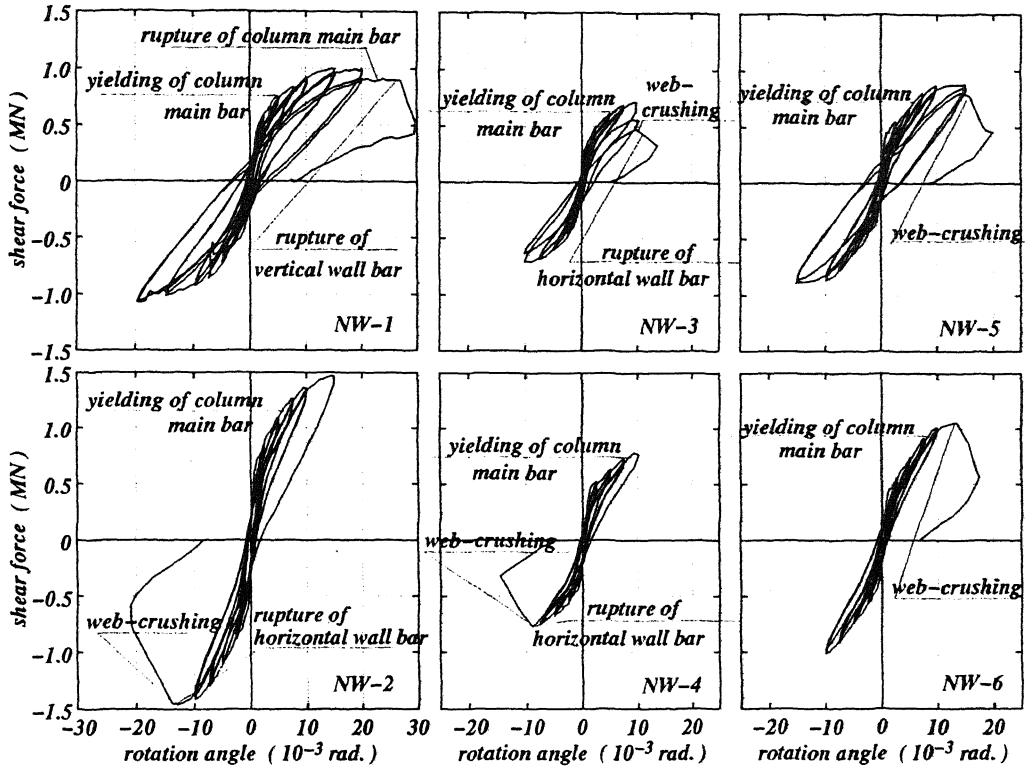

Figure 4 Overall hysteresis relations

Table 3 Measured resistances and deformations

	flexural cracking	diagonal cracking	column bar yielding	wall bar yielding	maximum strength
NW-1	323 (0.80)	529 (1.80)	760 (5.01)	911 (10.1)	1062 (19.7)
NW-2	526 (0.56)	715 (1.24)	1151 (5.58)	1353 (10.0)	1468 (14.9)
NW-3	191 (0.27)	418 (1.65)	628 (5.80)	711 (9.10)	717 (9.90)
NW-4	253 (0.69)	492 (1.79)	741 (8.40)	---	784 (9.30)
NW-5	190 (0.15)	453 (0.97)	731 (6.05)	821 (8.38)	900 (15.2)
NW-6	241 (0.50)	468 (1.73)	937 (8.49)	1014 (9.97)	1056 (13.4)

unit of resistance in kN (corresponding deformation in $x10^{-3}$ rad.)

(the lateral load level). The horizontal displacements and axial deformations measured at several nodes of the boundary columns, from which flexural and shear deformations were derived. Strain gauges are placed in the reinforcing bars at the selected locations in the wall panel and boundary columns.

3 TEST RESULTS

3.1 Failure modes

Observed failure modes of the specimens NW-1 and NW-2 in the first phase were different from each other. At the deflection angle of R=1/100, small part of the cover concrete at the compression side of the boundary column started to spall off in the specimen NW-1, which was not observed in NW-2. Ductile and stable behaviors were observed within the loading cycles of R=1/50 for NW-1 and R=1/100 for NW-2. Brittle failure occurred at different deformation levels for the two specimens: The tensile column and wall longitudinal bars in the specimen NW-1 ruptured at R=1/40; The specimen NW-2 failed in web-crushing and almost simultaneous rupture of lateral shear reinforcement in the wall panel at R=-1/67. Both specimens sustained the constant gravity load after the failure.

In the second phase tests, similar cracking patterns were observed in the four specimens as that of NW-1 in the first phase. Shear cracks observed in NW-3 and NW-4 were wider than those in NW-5 and NW-6 due to the lower web reinforcement ratios.

The four specimens failed at different ductility level in a similar mode of web-crushing: The specimen NW-3 failed in rupture of lateral web reinforcement and web-crushing of side and lower part during the second cycle of loading with the amplitude of R=1/100; NW-4 in the same mode of NW-3 during the first cycle of R=1/100; NW-5 failed in web-crushing at the center and lower part after the loading cycles of R=1/67 and in the way to R=1/50; NW-6 in the same mode of NW-5 after the loading cycles of R=1/100 and at a little less than R=1/67.

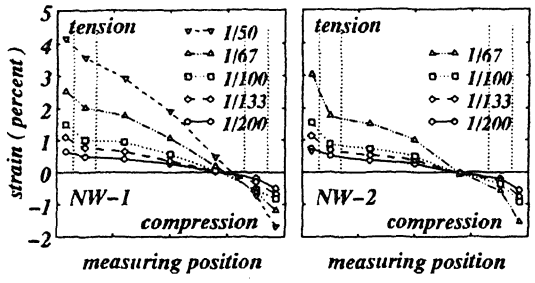

(a) axial strains at base

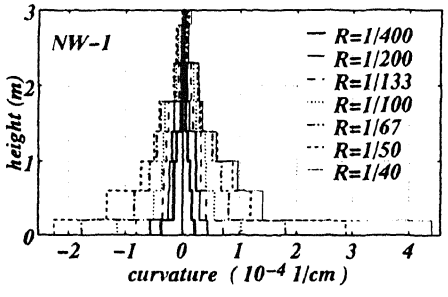

(b) curvatures along height

Figure 5 Axial strain and curvature distributions

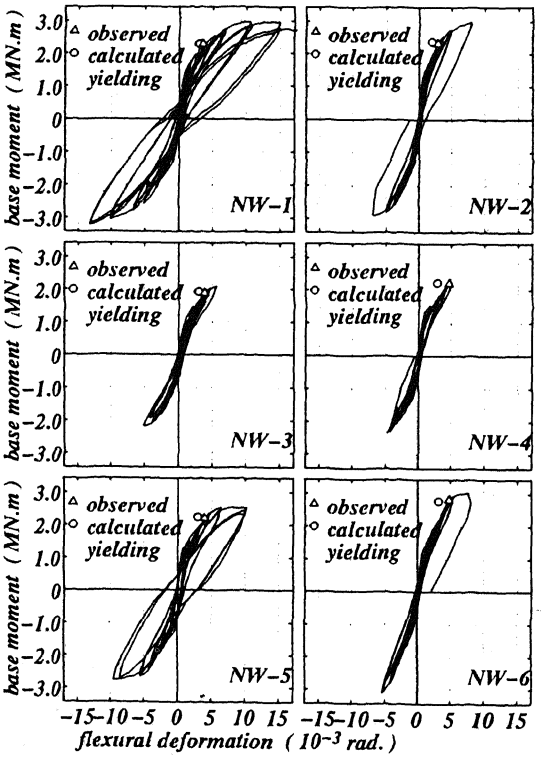

Figure 6 Base moment versus flexural deformations

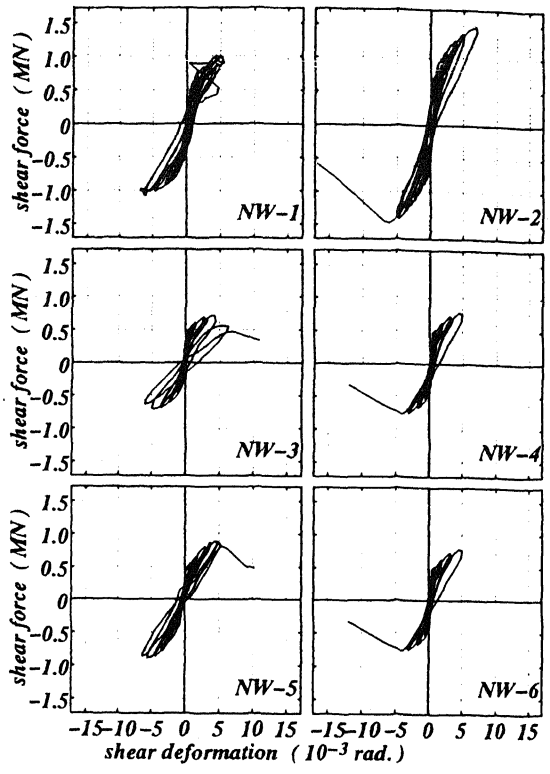

Figure 7 Shear force versus shear deformations

3.2 Hysteresis relations

The relations between the shear force and the overall lateral deflection at the top of the wall panel (loading level) are shown in Figure 4. Pinching behavior with relatively low energy dissipation, which may be caused by the small inelastic deformation of reinforcing steel and high axial load level, was observed in the relations.

Measured resistances and corresponding deformations are listed in Table 3, at which flexural cracking, diagonal shear cracking, yielding of column bar and wall longitudinal bars and web-crushing were observed.

Axial strain distribution along the wall base measured by displacement gauges within 15 cm are shown in Figure 5(a) for the first phase tests. Linear strain distribution is observed. The maximum axial strains at the compression side were about 0.8% in the specimen NW-1 and 0.5% in NW-2, which explained minor damage of the column in NW-2. The axial force carried by the column in specimen NW-2 was estimated to be smaller because the wall panel carried mode as the diagonal compressive force. Tensile yielding of the main bars in the column was observed first at R=1/200 in specimen NW-1 and at R=1/133 in NW-2.

Curvature distribution along the height of the wall calculated from the column axial deformations is shown in Figure 5(b). Linear distribution is observed within yielding at 1/200, while it concentrates at lower part at larger deformations.

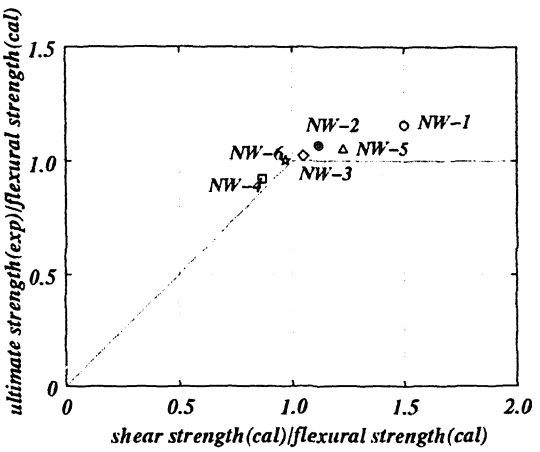

Figure 8 Observed and calculated ultimate strengths

Flexural deformation was obtained by integrating the curvatures from the column axial deformations along the wall height. Hysteresis relations of the flexural deformations and the base moment are shown in Figure 6. Flexural deformations at column yielding are indicated in the figure with those calculated by the flexural theory presented in the next section.

By taking the flexural deformation from the overall deformation, the remainder was defined as the shear deformation. Hysteresis relations of the shear deformation and the shear force are shown in Figure 7. Shear deformations at the web-crushing are around 0.65 and 0.5 percent for the phase-one and phase-two specimens, respectively, while the flexural deformations vary in relation to the deformation capacity.

4 EVALUATION OF TEST RESULTS

4.1 Flexural and shear strengths

Ultimate flexural strengths of the specimens were calculated by the following equation (1), which based on a flexural theory and is practically used as an approximate design equation in Japan:

$$M_u = A_t \sigma_y l_w + 0.5 A_w \sigma_{wy} l_w + 0.5 N l_w \qquad ...(1)$$

where,

A_t, σ_y : total area and yield strength of longitudinal reinforcing bars in tensile boundary column
A_w, σ_{wy} : total area and yield strength of longitudinal reinforcing bars in wall panel
l_w : total width of shear wall including boundary columns (=150cm)
N : axial load
σ_B : compressive strength of concrete

The ratios of the measured ultimate moments at the base of the specimens to the calculated as above were 1.0 through 1.15, except for NW-4, which failed in web-crushing right after yielding of column main bars.

The shear failure due to web-crushing of concrete was observed in the specimens except for NW-1 after flexural yielding at deflection angles of R=1/133 through 1/67. The shear strengths of the specimens were also investigated by the following equations (2) through (8) based on a plastic theory combining arch and truss shear resistance mechanisms. The equations are proposed by the design guidelines published by the Architectural Institute of Japan (Architectural Institute of Japan, 1990):

$$V_u = t_w l_{wb} p_s \beta_{sy} \cot\phi + \tan\theta (1-\beta) t_w l_{wa} \nu \sigma_B/2 \qquad ...(2)$$

$$\tan\theta = \sqrt{(h_w/l_{wa})^2 + 1} - h_w/l_{wa} \qquad ...(3)$$

$$\beta = (1+\cot^2\phi) p_s \sigma_{sy}/(\nu \sigma_B) \qquad ...(4)$$

where,

t_w : thickness of wall panel (=8cm)
h_w : height of wall (=300cm and 200cm)
p_s, σ_{sy} : ratio and yield strength of horizontal shear reinforcement in wall panel ($p_s \sigma_{sy} = \nu \sigma_B/2$)
σ_B : compressive strength of concrete
ϕ : angle of compressive strut in truss mechanism
θ : angle of compressive strut of arch mechanism

Equivalent widths of wall panel in truss and arch mechanisms, l_{wb} and l_{wa}, are given as design formulae in the guidelines including effective length of boundary columns. Here, the total width was assumed simply for both of them as: $l_{wa}=l_{wb}=170$cm.

Strut angle of truss mechanism ϕ is tentatively assumed as 45 degrees in the guidelines, that is:

$$\cot\phi = 1.0 \qquad ...(5)$$

However, it is also indicated that the value can be assumed in slender members up to: $\cot\phi = 2.0$. Here, the value is tentatively assumed as:

$$\cot\phi = 1.5 \qquad ...(6)$$

because the value corresponded to the inclination of the dominating shear cracks observed in the tests.

Effective factor of compressive concrete strength ν is also given in the guidelines as follows:

$$\nu = 0.7 - \sigma_B/2000 \qquad ...(7)$$

However, this equation is not applicable and gives apparently low value for ultra-high strength concrete, which has been found after the first phase test. The following equation (8) proposed in a draft of CEB-FIP Model Code in 1987 is tentatively adopted here:

$$\nu = 1.7 \sigma_B^{-1/3} \qquad ...(8)$$

The factors calculated as above are about 0.38 and 0.44 for the first and second phase test series, respectively.

The observed and calculated shear strengths for all

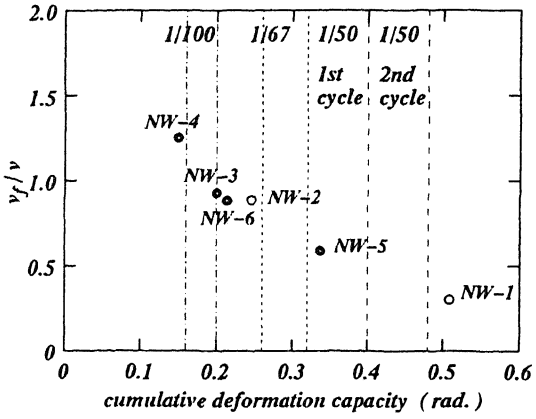

Figure 9 Deformation capacity in relation to the concrete strut strength required at flexural capacity

the specimens are plotted in Figure 8. Both are normalized by the calculated flexural strengths. It should be noted that the observed shear strength was obtained relatively at large deformation level, at which effective concrete strength is supposed to decrease due to tensile strain. Because the observed strengths are larger than the calculated in both cases, it may be assumed that the strut angle of the truss mechanism be smaller than 45 degrees. This value should be investigated further with the combination of the effective strength.

4.2 Yield and ultimate deformations

In a design method which is based on ductile behavior and uses a nonlinear frame analysis, it is important to evaluate theoretically not only the strengths level but also the inelastic deformations at critical points, such as yielding and crushing. Here, flexural deformation at yielding of column bar, shear deformation at web-crushing are calculated theoretically. Also the ultimate deformation capacity is investigated through the shear resistance mechanism.

Flexural deformation at flexural yielding may be calculated by the flexural theory. Yield curvature was calculated by using a simple concrete and steel model. Because linear curvature distribution along the height of the wall may be assumed as is observed in Figure 5(b), the yielding deflection angle R_f at the top of the wall by the flexural deformation can be calculated using yielding curvature at the base ϕ_y as:

$$R_f = \phi_y h_w / 3 \qquad ...(9)$$

Calculated yielding resistance and deformations are plotted with small circles in Figure 6, which generally agrees with the observed (triangles in the figure), but a little smaller in NW-4 and NW-6.

Shear deformations at web-crushing can be formulated using diagonal compression strain ε_{cu} of concrete strut as:

$$R_s = (\cot\phi + \tan\phi)\, \varepsilon_{cu} \qquad ...(10)$$

If ecu is assumed as the strains at compressive strength of concrete from the material tests, 0.30 for the first phase and 0.25 percent for the second phase (Table 2(b)), and $\cot\phi = 1.5$ is assumed, R_s are calculated as 0.65 and 0.54 percent, respectively. The observed shear deformations at web crushing are around 0.65 and 0.50 percent in the first and the second phase, as shown in Figure 7, which are close to the calculated.

The ultimate deformation capacity, which is defined as the cumulative deformation until the shear resistance level decayed to the 80 percent of the observed maximum strength, are plotted in Figure 9 for the six specimens in relation to the following calculated factor for the deformability.

Web-crushing after flexural yielding may due to the loss of the shear capacity, which is caused by the reduction of concrete strength due to the flexural and shear cracking or the tensile deformation in orthogonal direction of the compressive concrete strut. Therefore, the calculated factor for the deformation capacity is defined as the ratio of the required concrete strut capacity at the flexural failure to the concrete strut capacity in the shear resistance (arch and truss) mechanism. In other words, the effective concrete strength v_f is calculated by which the shear strength using eqs.(2)-(4) become equal to the shear at the flexural strength using eq.(1). Then the factor is defined as the ratio of v_f to the basic value of v by eq.(8).

Clear relationship is obtained that the lower the effective concrete strength required at the flexural capacity is, the higher the deformation capacity becomes, which may be used in the ultimate-state design of a ductile flexural shear wall to ensure the deformation capacity higher than required during an earthquake response.

5 CONCLUSIONS

The following conclusions are derived from the tests and analyses of ultra-high strength reinforced concrete shear walls:

1. Ductile shear walls in flexural behavior can designed using ultra-high strength reinforced concrete. However, obvious pinching behavior was observed in the hysteresis relations, which should be taken into account in design and analysis.

2. Observed ultimate and yield flexural strengths can be predicted by the flexural theory.

3. The shear design equation may conservative for the ultra-high strength reinforced concrete shear walls. A modification is presented for the effective factor and the angle of concrete strut in the truss mechanism.

4. The flexural deformations at yielding can be estimated by a flexural theory. The shear deformations at web-crushing corresponded to those caused by the ultimate compressive strains in the concrete strut.

5. The cumulative deformation capacity was clearly related to the calculated margin of the concrete strut strength in the shear resistance mechanism.

ACKNOWLEDGEMENTS

The study is being conducted at Structural Laboratory, Yokohama National University, and is sponsored by the "New RC project," Ministry of Construction, Japan. The authors gratefully acknowledge the contributions of Mr. Hiroshi Kuramoto, research associate and Messrs. Kiyoomi Kanemoto, Mitsuhiko Masuo, Hakuei Ishida, formerly undergraduate students, Yokohama National University, in fabrication and testing of the specimens.

REFERENCES

Architectural Institute of Japan(AIJ), 1990. *Design guidelines for earthquake resistant reinforced concrete buildings based on ultimate strength concept (in Japanese).* Architectural Institute of Japan, Tokyo